SYSTEM ANALYSIS OF *PHYCOMYCES* LIGHT-GROWTH RESPONSE

Wavelength and Temperature Dependence

PROMOD PRATAP, ANURADHA PALIT, AND EDWARD D. LIPSON
Department of Physics, Syracuse University, Syracuse, New York 13244-1130

ABSTRACT The light-growth response of the *Phycomyces* sporangiophore was studied further with the sum-of-sinusoids method of nonlinear system identification. The first- and second-order frequency kernels, which represent the input-output relation of the system, were determined at 12 wavelengths (383–529 nm) and 4 temperatures (17°, 20°, 23°, and 26°C). The parametric model of the light-growth response system, introduced in the preceding paper, consists of nonlinear and linear dynamic subsystems in cascade. The model parameters were analyzed as functions of wavelength and temperature. At longer wavelengths, the system becomes more nonlinear. The latency and the bandwidth (cutoff frequency) of the system also vary significantly with wavelength. In addition, the latency decreases progressively with temperature (Q_{10} = 1.6). At low temperature (17°C), the bandwidth is reduced. The results indicate that about half of the latency is due to physical processes such as diffusion, and the other half to enzymatic reactions. The dynamics of the nonlinear subsystem also vary with wavelength. The dependence of various model components on wavelength supports the hypothesis that the light-growth response, as well as phototropism, are mediated by multiple interacting photoreceptors.

INTRODUCTION

In the previous paper (Pratap et al. 1986), we applied the sum-of-sinusoids method (Victor and Shapley, 1980) of nonlinear system identification to the light-growth response of *Phycomyces*. With this method, we determined the first- and second-order frequency kernels of the wild-type strain under standard conditions (wavelength 477 nm and log-mean intensity, $I_0 = 10^{-4}$ W m^{-2}). From these kernels, we derived a nonlinear model in terms of subsystems governed by first- or second-order linear differential equations (filters) and a static nonlinear element (a squarer). These subsystems form an internal model of the light-growth response.

In this paper, we apply the sum-of-sinusoids method to analyze how the light-growth response depends on wavelength and temperature. The wavelength dependence is of special interest, in view of recent action spectroscopy studies of phototropism (Galland and Lipson, 1985*a*, *b*) and related studies of the wavelength dependence of adaptation (Galland et al., 1984). A major conclusion of those studies was that *Phycomyces* phototropism is mediated by multiple interacting photoreceptors. The blue-light responses of *Phycomyces* sporangiophores—the light-growth response and phototropism—evidently share a common photoreceptor system, in view of their similar action spectra (Delbrück and Shropshire, 1960) and their similar reductions of sensitivity in night-blind mutants (Bergman et al., 1973). In the context of the model introduced in Pratap et al. (1986), we have investigated the dynamics of the light-growth response as a function of wavelength. The dependence of the model parameters on wavelength helps us to distinguish which components of the model are associated with the photoreceptor system.

The light-growth response is known to depend on temperature (Foster and Lipson, 1973). Over the range from 15° to 25°C, the latency was found to decrease progressively. Here, we have measured the frequency kernels at four temperatures, and evaluated the dependence of the latency and other model parameters on temperature.

MATERIALS AND METHODS

The experimental protocols were similar to those followed in the preceding paper. To obtain monochromatic light from the tungsten halogen lamp, we used interference filters (Balzers B-40, 9–12-nm bandwidth; Rolyn Optics, Covina, CA). The experiments on wavelength dependence were all performed at 20°C. The log-mean intensity I_0 (defined by $\log I_0 = \langle \log I \rangle$, where the angle brackets represent a time average) at each wavelength is given in Table I. These intensities were chosen on the basis of the photogravitropic equilibrium action spectrum of Galland and Lipson (1985*a*) so as to provide a subjective intensity equivalent to 10^{-4} W m^{-2} of 450 nm light.

The component frequencies of the sum-of-sinusoids stimulus were all multiples of the fundamental frequency $f_0 = 0.0037$ min^{-1}. Two sets of frequency multipliers were used. One set (same as in Pratap et al., 1986)

Address correspondence and reprint requests to Edward D. Lipson, Department of Physics, Syracuse University, Syracuse, NY 13244-1130.

TABLE I
COMPARISON OF RESULTS OF SUM-OF-SINUSOIDS EXPERIMENTS AT 12 WAVELENGTHS

Wavelength	Log-mean intensity* ($\times 10^4$)	No. of expts.	Mean growth rate‡	MSE of model response§			Percentage improvement‖	Strength of nonlinearity¶
				Zero order	First order	Second order		
nm	*W m*$^{-2}$		*μm min*$^{-1}$	*μm min*$^{-2}$	%	%	%	decade^{-2}
383	2.1	6	34.4 ± 4.1	64.3	21.5	12.6	41.4	0.30
394	2.1	6	40.6 ± 2.2	56.5	22.9	13.2	42.4	0.28
414	2.3	6	40.6 ± 4.6	81.7	18.3	11.8	35.5	0.25
423	2.1	5	42.4 ± 2.1	41.1	25.6	19.0	25.8	0.18
431	2.0	5	36.7 ± 1.4	55.4	20.0	14.1	29.5	0.24
446	1.5	5	37.4 ± 3.5	44.4	26.4	14.3	45.8	0.46
469	1.3	5	37.5 ± 4.2	43.5	27.5	15.0	45.5	0.55
477	1.0	15	36.6 ± 2.7	41.9	30.4	15.5	49.0	0.58
487	1.3	6	35.8 ± 2.4	41.7	22.5	10.9	51.6	0.62
491	2.0	8	41.0 ± 1.7	31.9	16.3	11.2	31.3	0.46
507	6.6	6	40.1 ± 1.3	35.7	18.6	13.2	29.0	0.58
529	300	5	35.9 ± 3.6	40.8	24.5	16.7	31.8	0.50

*The log-mean intensity is equivalent to 1.0×10^{-4} W m^{-2} of 450 nm light, according to the photogravitropic equilibrium action spectrum of Galland (1983).
‡Mean growth rate of sporangiophores. The error values represent standard errors. The growth rate does not depend significantly on wavelength (chi-square = 12.9, which is well below the value of $\chi^2_{11,.05} = 19.7$ at the 5% significance level with 11 degrees of freedom.
§Mean-square errors (MSE) between experimental and model response records. MSE for zero-order model (h_0) is in absolute units. MSEs for first-order (h_1) and second-order (h_1, h_2) models are given as percentages of zero-order MSE.
‖Percentage improvement of second-order model over first-order model. This is the difference between the MSEs of the first- and second-order model responses as a percentage of the MSE of the first-order model response.
¶Strength of nonlinearity is the ratio between the mean-square value of the second- and the first-order kernels.

was {7, 17, 33, 53, 71, 80, 92, 115, 147, 192, 249, 297, 338, 380, 473}. The other set was {7, 15, 31, 63, 127, 255, 511, 1,023} (Victor and Shapley, 1980). First- and second-order kernels were determined with the first set at seven wavelengths: 414, 431, 446, 469, 477, 487, and 507 nm. First-order kernels alone were determined with the second set at these wavelengths and at five additional wavelengths: 383, 394, 423, 491, and 529 nm. At the seven wavelengths where both sets were used, the first-order kernels were identical within errors.

The experiments to study the temperature dependence were performed at 17°, 20°, 23°, and 26°C with 477 nm light and with $I_0 = 10^{-4}$ W m^{-2}. This value of I_0 is subjectively equivalent to 10^{-4} W m^{-2} of 450 nm light (see above). The temperature dependence experiments employed only the first set of frequency multipliers.

RESULTS

Table I evaluates the relative contributions of the first- and second-order kernels to the experimental response at 12 wavelengths. The mean-square error (MSE) of the first-order model response is typically 23% of the zero-order MSE, which is itself just the variance of the experimental response (Pratap et al., 1986, for explanation). On the average, the MSE of the second-order model response is 14% of the response variance. For all 12 wavelengths, inclusion of the second-order contribution provides significant improvement in the MSE.

The last two columns of Table I provide two measures of how nonlinear the system is at different wavelengths: (*a*) the percentage improvement of the second-order external model over the first-order model; and (*b*) the strength of nonlinearity, defined as the ratio of the mean-square value of the second-order kernel to that of the first-order kernel (the latter measure is expected to be more robust, because it is unbiased by random noise in the experimental response). The percentage improvement of the second-order model over the first-order model correlates fairly well with the strength of nonlinearity; specifically, the extreme values of both measures coincide (i.e. the system appears to be least nonlinear at 423 nm and most nonlinear at 487 nm). There is a pronounced jump in the strength of nonlinearity between 431 and 446 nm; the average strength of nonlinearity for wavelengths above 440 nm is about twice that for wavelengths below 440 nm (0.25 vs. 0.54 decade^{-2}).

Fig. 1 *a* shows the amplitude of the first-order frequency kernel $H_1(f)$ at three representative wavelengths (414, 477, and 507 nm). The solid lines are based on the first-order kernel of the internal, analytical model described in Pratap et al. (1986). The parameters of the internal model were obtained with a combined least-squares procedure, in which the internal model response at the component frequencies and combination frequencies was fit to the Fourier transform of the experimental response at these frequencies. In the model, the amplitude of $H_1(f)$ is proportional to f at low frequencies and to f^{-4} at high frequencies. On a double-logarithmic plot (Fig. 1), the amplitude of H_1 thus has a slope of approximately 1 at low frequencies and -4 at high frequencies (see Lipson, 1975*a*).

For the three representative wavelengths in Fig. 1, the frequency kernels (*left*) appear similar in shape. However, the amplitude (i.e. absolute value) of the complex-valued frequency kernel contains only half the information; the other half is contained in the phase (not shown). To convey the complete information in a simple way, we have transformed the complex-valued frequency kernels to the time domain with a Fast Fourier Transform algorithm. These

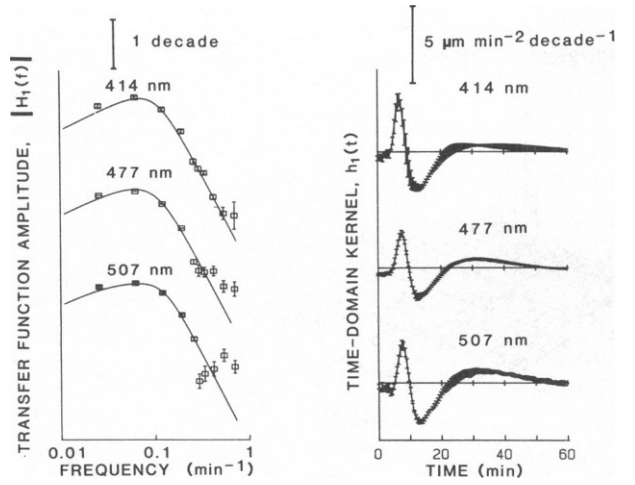

FIGURE 1 First-order kernels for three representative wavelengths (414, 477, and 507 nm). (*Left*) amplitude (absolute value) of complex-valued frequency-domain kernels shown on double-logarithmic axes. This amplitude includes only half of the information of the kernel; the remainder is in the phase (not shown). (*Right*) Averages of corresponding time-domain kernels of individual experiments. All experiments were performed at subjective intensities equivalent to $I_0 = 10^{-4}$ W · m^{-2} at 450 nm according to the wild-type photogravitropic-equilibrium action spectrum of Galland, 1983). The temperature was 20.0 ± 0.5°C. The experimental points in the plots to the left are shown with error bars (standard errors for 5–6 experiments each). The solid line in these plots represent the first-order frequency kernel of the nonlinear model described in Pratap et al., 1986. This first-order model kernel is

$$W(s) = \beta_L e^{-st_0}\left[\frac{s}{s + 2\pi f_{L1}}\right] \cdot \left[\frac{(2\pi f_{L2})^2}{s^2 + (2\alpha_L)(2\pi f_{L2})\, s + (2\pi f_{L2})^2}\right]^2,$$

where s is the Laplace transform variable, β_L is the overall gain factor, f_{L1} is the cutoff frequency of the first-order high-pass filter, f_{L2} and α_L are the cutoff frequency and damping coefficients of the two identical second-order low-pass filters, and t_0 is the latency. The second-order model kernel is $W(s_1 + s_2)P(s_1)P(s_2)$, with

$$P(s) = \frac{\beta_{N1}}{s^2 + (2\alpha_{N1})(2\pi f_{N1})s + (2\pi f_{N1})^2} + \frac{\beta_{N2}s}{[s^2 + (2\alpha_{N2})(2\pi f_{N2})s + (2\pi f_{N2})^2]^n},$$

where β_{N1} and β_{N2} are overall gain factors for the two filters, f_{N1} and f_{N2} are the cutoff frequencies, α_{N1} and α_{N2} are the damping coefficients, and n is an exponent in the second filter. The time-domain kernel of each experiment was obtained by interpolation and Fourier transformation of the corresponding frequency kernels.

kernels (Fig. 1 *b*) resemble the Wiener kernels obtained by the white-noise method (Lipson, 1975*a*, *b*; Poe and Lipson, 1986). As expected theoretically, the time-domain kernels (by either method) resemble the light-growth response to pulse stimuli of small strength. The kernels exhibit a latency of ~4 min, a maximum at 8 min, and a minimum (undershoot) at ~13 min. After a slight overshoot, the kernels decay to zero within an hour.

Fig. 2 shows the amplitudes of the second-order frequency kernels at three wavelengths for the same experiments as in Fig. 1. Because the kernel amplitude is negligible over most of the sum quadrant (see Pratap et al., 1986), only the difference quadrant is displayed in each case. The experimental kernels (Fig. 2 *a*, *b*, and *c*) are generally similar for the three wavelengths. For each wavelength shown, the kernel has peaks at the frequency pairs (0.29 min^{-1}, 0.34 min^{-1}; intermediate frequencies near the center of the plot) and (0.03, 0.06 min^{-1}; low frequencies to the right of the plot). As discussed in Pratap et al. (1986), the fact that the second-order kernel is not flat along the difference diagonal indicates that the nonlinearity is dynamic.

Although the positions of the peaks are independent of wavelength, their relative heights vary. For the kernels at 414 and 477 nm, the peaks at the intermediate-frequency pair (near the center of the plot) are larger than the peaks at the low-frequency pair, but the peaks are almost equal for the 507-nm kernel. These differences are reflected in the model kernel parameters estimated from the fits of the model to the data (see below).

Both frequencies of the intermediate-frequency pair are well above the cutoff frequency of the first-order kernel (f_c = 0.11 min^{-1} for 477 nm; see Pratap et al. (1986)), but the combination frequency (0.05 min^{-1}, i.e. 0.34–0.29 min^{-1}) is below the cutoff. As discussed in Pratap et al. (1986), the large amplitude of the second-order kernel at high frequencies (and close to the difference diagonal) implies that the nonlinearity lies towards the input of the system.

For each wavelength, a nonlinear least-squares fit of the model response to the experimental response yielded estimates of the model parameters. For the three wavelengths shown, the amplitudes of the model kernels (Figs. 2 *d–f*) reproduce the main features of the experimental kernels. The peaks appear at the same frequency pairs and with similar relative heights to those in the experimental kernels.

In Fig. 3, the parameters of the first-order model kernel (*a–e*) and the second-order model kernel (*f–l*) are shown as functions of wavelength. We have tested the hypothesis that each parameter is constant with respect to wavelength by fitting these parameter values (with error weighting) to a straight line with zero slope (i.e., to a constant). The normalized chi-square of the fit (see Pratap et al., 1986), serves as a goodness-of-fit parameter (Table II). At the 5% significance level, the first-order kernel parameters, β_L, f_{L1} and α_L, fit well to the horizontal lines as shown, but f_{L2} and t_0 fail to fit to a constant even at the 1% significance level. The cutoff frequency f_{L2} is high in the near ultraviolet (383 and 394 nm), and appears relatively constant at higher wavelength. The system represented by the second-order low-pass filter operates faster in the ultraviolet than in the blue. The parameter f_{L2} and the response variance (MSE of the zero-order model response; Table I) vary similarly

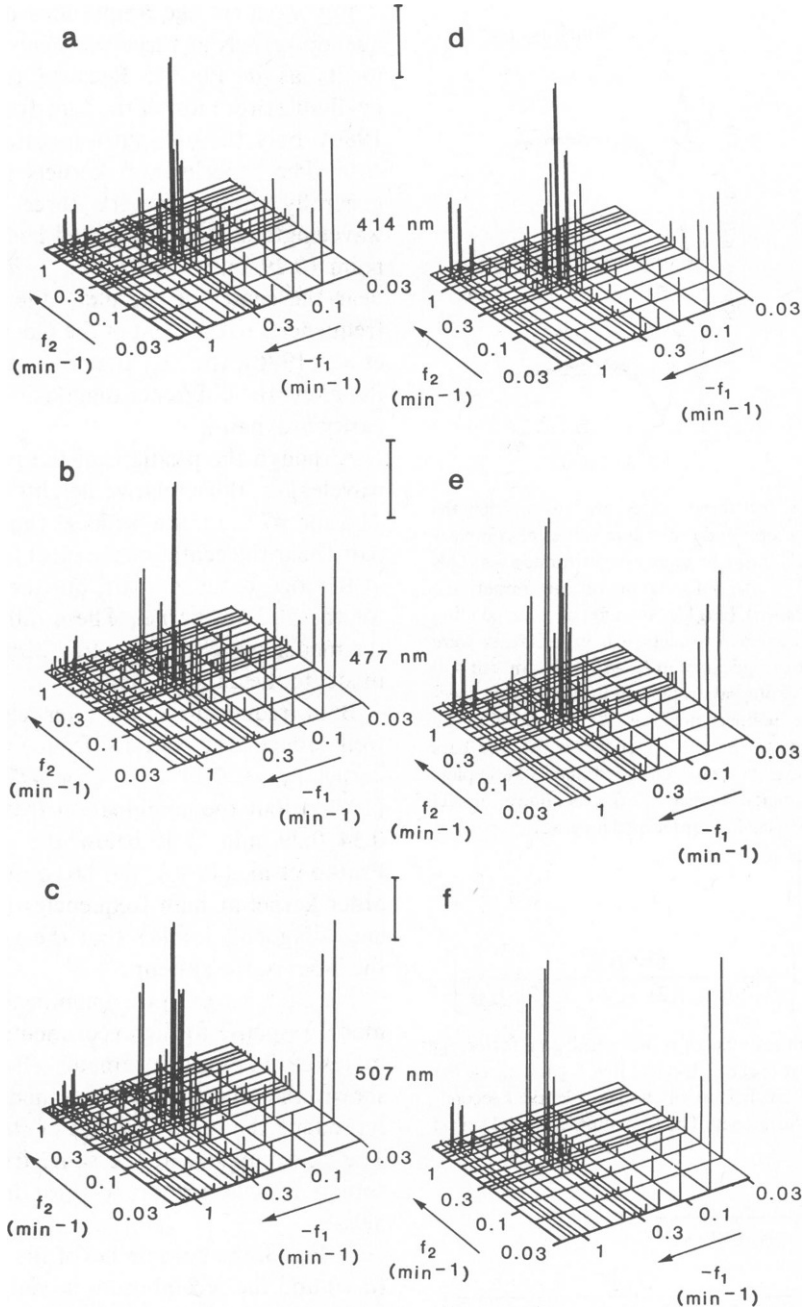

FIGURE 2 Magnitude of the second-order frequency kernels in the difference quadrant. Same experiments as in Fig. 1. Kernels calculated from experimental data are shown at *left* (*a, b, c*). Kernels of the internal model are shown at *right* (*d, e, f*).

with wavelength. The latency t_0 has a relative maximum at 394 nm, a minimum at 423 nm, and a sharp maximum at 487 nm. The system is slower by about 0.5 min at 487 nm than at 477 or 491 nm.

The second-order (nonlinear) parameters, f_{N1}, α_{N1}, α_{N2} and n, do not vary significantly with wavelength (5% significance level), but β_{N1}, β_{N2} and f_{N2}, do. The gain factor β_{N1} tends to increase with wavelength. It is almost zero at 446 nm, but increases to over 0.2 min^{-2} decade$^{-1/2}$ above 500 nm, with a slight local minimum at 487 nm. The other gain factor β_{N2} has a single peak around 480 nm. The cutoff frequency f_{N2} shows an overall increase with wavelength, with a local maximum at 487 nm. The variation of f_{N2} with wavelength parallels the variation of β_{N1}. This filter (designated P_2 in Fig. 4 *b* of Pratap et al., 1986) thus tends to operate faster at longer wavelength. The gain factor β_{N1} of the low-pass filter (designated P_1 in Fig. 4 *b* of Pratap et al., 1986) reflects approximately the strength of nonlinearity (Table I): larger at longer wavelengths.

Fig. 4 shows the temperature dependence of the parameters for the first-order model kernel. The parameters β_L, f_{L1} and α_L are independent of temperature over the range

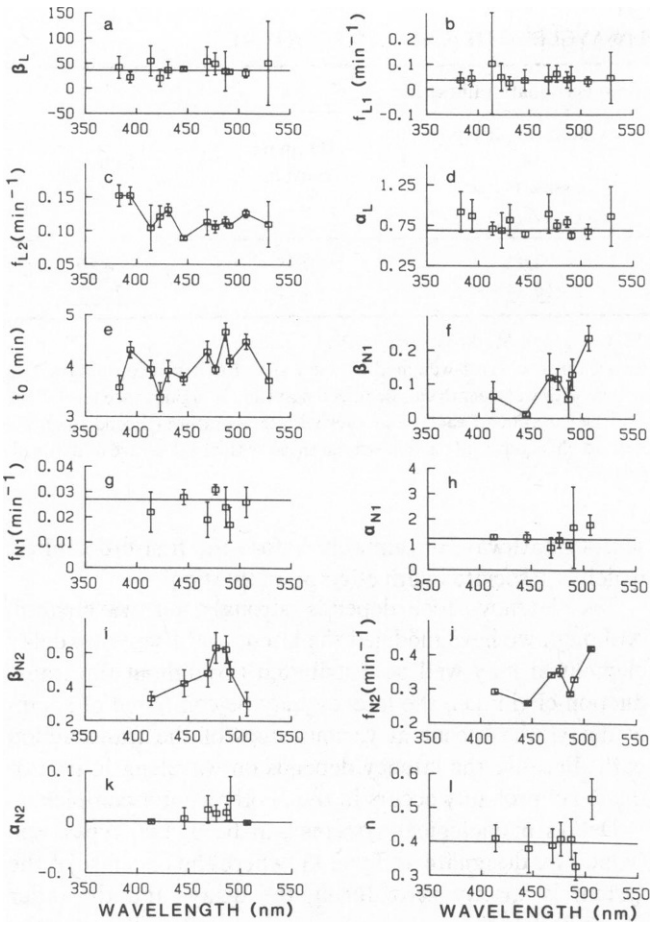

FIGURE 3 Internal model parameters as functions of wavelength. Parameters of linear subsystem: an overall gain factor β_L (*a*) cutoff frequency f_{L1} (*b*) of first-order high-pass filter, cutoff frequency f_{L2}, (*c*) and damping constant α_L (*d*) of second-order low-pass filters, and latency t_0 (*e*). Parameters of nonlinear subsystem: gain factor β_{N1} (*f*), cutoff frequency f_{N1} (*g*), and damping constant α_{N1} (*h*), of the second-order low-pass filter; gain factor β_{N2} (*i*), cutoff frequency f_{N2} (*j*), damping constant α_{N2} (*k*), and exponent n (*l*) of the high-pass filter. Because the parameters f_{L2}, t_0, β_{N1}, β_{N2} and f_{N2} vary significantly with wavelength, the points in the plots have been joined for clarity; for the other parameters, the best-fit straight line has been shown instead. The units of β_L are $\mu m \cdot min^{-1}$ decade^{-1}. The units of β_{N1} are min^{-2} decade$^{-1/2}$ and of β_{N2} are min^{-2n+1} decade$^{-1/2}$. The second-order kernels of the experiments done with the first set of frequency multipliers (see Materials and Methods) were analyzed for the second-order kernel parameters.

17–26°C; (5% significance level). The parameters f_{L2} and t_0 do depend significantly on temperature; the departure of t_0 from a constant is highly significant (1% significance level). As expected, the latency decreases with temperature approximately linearly. A fit to a straight line yields a slope of -0.172 ± 0.018 min/°C. From this best-fit line, we have derived a $Q_{10} = 1.6 \pm 0.1$ (ratio of parameter values at two temperatures 10°C apart, here 17° and 27°C). The parameter f_{L2} shows little variation at the three highest temperatures (20°, 23°, and 26°C), but the low temperature (17°C) value is significantly lower. Because f_{L2}, the cutoff frequency of the two identical second-order low-pass filters, represents the bandwidth of the system, this result indicates that the rate-limiting kinetics become significantly slower at this low temperature.

DISCUSSION

With the sum-of-sinusoids method, we have determined the first- and second-order frequency kernels of the light-growth response system at 12 wavelengths and at four temperatures. These kernels, which represent the input-output relation of the system, can be readily interpreted by system analysis methods. Specifically, we have analyzed the kernels in the framework of a parametric model introduced in the previous paper (Fig. 4 *b* and Eq. 5).

Linear Analysis

The model consists of a dynamic linear subsystem preceded by a dynamic nonlinear subsystem. The linear subsystem can be decomposed into the following elements (Lipson, 1975*a*): a first-order high-pass filter, two identical second-order low-pass filters, a gain element, and a delay element. Lipson (1975*a*) associated the high-pass filter with adaptation kinetics according to the model of Delbrück and Reichardt (1956), and found good agreement between the time constant of dark adaptation and the time constant (given by $1/(2\pi f_{L1})$) of the high-pass filter. With the white-noise method, Lipson (1975*a*) found this time constant to be 4.2 ± 1.5 min for $I_0 = 10^{-2}$ W m^{-2} and wavelength 488 nm. A weighted average of f_{L1} from our values at the 12 wavelengths (Fig. 3), gives a value of $f_{L1} = 0.035 \pm 0.009$ min^{-1}, which translates to a time constant of 4.6 ± 1.2 min, in agreement with the above value, notwithstanding the differences in wavelengths and intensity ranges. For our data, the log-mean intensities are equivalent to $I_0 = 10^{-4}$ W m^{-2} at 450 nm.

Insofar as the first-order high-pass filter represents adaptation kinetics, the apparent constancy of f_{L1} with wavelength (Fig. 3) suggests that adaptation is independent of wavelength. At first sight, this seems to contradict the recent finding of Galland et al. (1984) that adaptation kinetics depend significantly on wavelength. However, there are some theoretical and practical aspects to adaptation in *Phycomyces* that must be considered (Lipson, 1975*a;* Lipson and Block, 1983; Galland et al., 1984). First, there are two types of adaptation in *Phycomyces:* (*a*) range adjustment of sensitivity (sensor adaptation), and (*b*) regulation of growth rate (effector adaptation). Second, there are two specific ways to measure adaptation: the light-growth response method (Delbrück and Reichardt, 1956; Lipson and Block, 1983) and the phototropic latency method (Galland and Russo, 1984; Galland et al., 1984). Both of these methods are directed at the large-scale range-adjustment aspect of adaptation, which occurs over the full range of 10^{10}:1 in light intensity. On the other hand, in the system analysis work with Gaussian white-noise and sum-of-sinusoids test stimuli, the dynamic range of these stimuli is limited to a few decades, so that one is essentially

TABLE II
TESTS OF PARAMETER VARIATION WITH WAVELENGTH AND TEMPERATURE

Condition*	Normalized chi-square values‡ for				
	Gain (β_L)	Cutoff frequency of high-pass filter (f_{L1})	Cutoff frequency of low-pass filter (f_{L2})	Damping constant (α_L)	Latency (t_0)
Wavelength	0.41	0.19	3.92	0.38	4.99
Temperature	0.96	0.93	16.94	2.11	26.77

*Parameters were determined at 12 wavelengths and 4 temperatures (listed in Materials and Methods; see also Figs. 3 and 4).
‡For each parameter, the normalized chi-square is obtained from the fit of a constant (i.e. error-weighted averaging) to the parameter values as a function of wavelength (first row). The hypothesis that each parameter does not vary with wavelength can be rejected at the 5% significance level if the normalized chi-square value exceeds 1.79 (11 degrees of freedom). Similarly, for the variation of each parameter with temperature (second row), the critical value of the normalized chi-square is 2.60 (3 degrees of freedom). Normalized chi-square values that exceed these critical values are underlined. The parameters f_{L2} and t_0 thus appear to depend on both wavelength and temperature.

confined to the growth-rate regulation phenomenon (although this regulation aspect can be dealt with in the context of linear system theory, the range adjustment of sensitivity is strictly a nonlinear phenomenon and would have to be addressed by second- and higher-order kernels). Moreover, the association in the present work of adaptation with a first-order high-pass filter, or pseudodifferentiator, specifically addresses growth-rate regulation. Thus, while Galland et al. (1984) showed that sensor adaptation depends on wavelength (and thus probably involves the photoreceptor system directly), we find that effector adaptation appears to be independent of wavelength. It is not surprising that growth-rate regulation should be governed by dark reactions well beyond the photoreceptor system.

Although the cutoff frequency f_{L1} of the first-order filter shows no dependence on wavelength, the cutoff frequency f_{L2} of the cascade of two identical second-order low-pass filters does depend significantly on wavelength (Fig. 3). This frequency is essentially the bandwidth of the entire system, and thus represents the rate constant(s) (except for a factor of 2π) of the rate-limiting reaction(s) of the light-growth response. The wavelength dependence of f_{L2} suggests that the second-order low-pass filters are coupled to the photoreceptor complex, and thus occur early in the sensory pathway, presumably before the first-order filter, which is associated with effector adaptation.

The latency, too, depends strongly on wavelength. Although we have modeled the latency as a separate delay element, it may well be distributed throughout the transduction chain; i.e., the latency may be composed of a sum of delays that occur at various steps of the transduction path. Because the latency depends on wavelength, part of the delay probably occurs in the photoreceptor complex.

Delays in biological systems can be of two types: one (which we designate as Type 1), where the response of the system is strictly zero during the delay, and the other (Type 2), where the response remains very small during the apparent delay. French (1980) proposed a model for a Type 1 delay in the visual system of the fly *Phormia regina*. He argued that such a delay can be introduced by queued diffusion, in which molecules arrive at the destination in the same order that they started. This queuing requires restricted movement of the molecules, for example in the microvilli of the rhabdom of the fly. The delays observed in the fly are of the order of milliseconds.

The delays observed in auxin-mediated cell elongation in higher plants are of the order of 10 min (Ray, 1977; Bowles and Northcote, 1974; Robinson and Kristen, 1982), com-

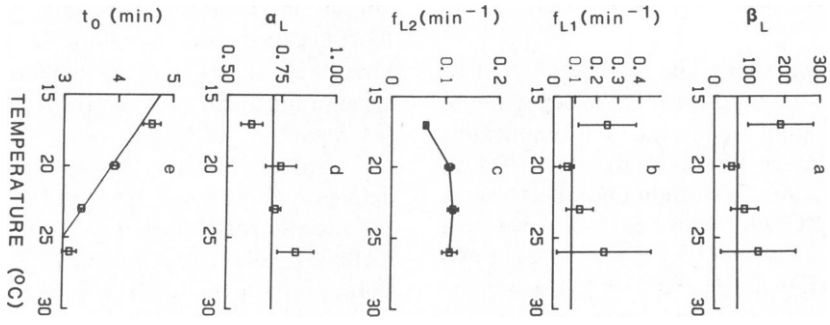

FIGURE 4 Temperature dependence of parameters for first-order kernel: gain factor (*a*), cutoff frequency of the first-order high-pass filter (*b*), cutoff frequency (*c*) and damping constant (*d*) of the second-order low-pass filters, and latency (*e*). The experiments were performed with 477 nm light at a log-mean intensity of 10^{-4} W m^{-2}. The units of β_L are μm min^{-1} decade^{-1}. The number of experiments at each temperature was as follows: 17° (6 experiments), 20° (15), 23° (7), and 26°C (6).

parable to the delays we observe. A model has been proposed for these delays that involves transport of protons and secretory proteins from the cisternal space of the endoplasmic reticulum to the cell exterior via the Golgi system (Ray, 1977). These delays would be of Type 2. Although Golgi systems have not been seen in *Phycomyces,* there are vesicles around the nuclei of the growing zones of stage I sporangiophores (young sporangiophores which have not yet produced the spherical sporangium) that appear to function as Golgi vesicles (Thornton, 1968).

Another way to produce a Type 2 delay is by a chemical cascade (Fuortes and Hodgkin, 1964). We have fitted the experimental first-order kernel to a cascade of n identical irreversible chemical reactions (results not shown). The best fit was obtained for a model with 12 sequential reactions. However, the transfer function (first-order kernel) for such a system would be of twelfth order, i.e., the system kinetics would obey a twelfth-order differential equation. From Bode analysis of the first-order kernel amplitude, Lipson (1975*a*) found that the light-growth response system is fifth order, with a delay of Type 1. Our data are fit far better by such a model than by the cascade model.

The cascade model does have the advantage, though, that it could explain the wavelength dependence of the latency. In this model, the latency depends strongly on the rate constants of the individual reactions. If some of these rate constants were dependent on wavelength, then the effective latency of the cascade would also vary with wavelength.

The latency may consist of both Type 1 (transport) and Type 2 (chemical cascade) delays. In Fig. 3 *e,* the latency t_0 varies from ~3.4 to 4.7 min over the wavelength range studied. If we assume that this variation is attributable only to Type 2 delays, then we can infer a lower limit of about 1.3 min for the contribution of Type 2 delays to the latency. The minimum latency of 3.4 min, similarly, serves as an upper limit for the contribution of Type 1 delays.

The variation of the latency t_0 with temperature is highly significant over the range tested. As expected, the latency decreases with increasing temperature. Foster and Lipson (1973) found that the latency of the light-growth response decreased with temperature; they deduced a Q_{10} value of 2.4. This value, however, was based on very limited data: two individual responses to pulse stimuli, one at 15° and one at 25°C; for the response at 25°C, there was a rather large uncertainty in what time value to take as the latency. In any case, with this Q_{10} value, the latency would seem to be attributable mainly to enzymatic reactions. In the present work, the latency has a Q_{10} of 1.6. This value is based on vastly more data (155 h, from 34 experiments each with effective duration 4.55 h; in the sum-of-sinusoids method, the entire experiment is analyzed uniformly) than the earlier value (half an hour). The difference between these two Q_{10} values may be due not only to experimental error, but also to the different experimental conditions and data analysis procedures. Foster and Lipson (1973) measured the latency directly from light-growth responses to pulse stimuli based on an adaptation level of 2×10^{-3} W m^{-2} (broadband blue light). On the other hand, we have extracted the latency as a parameter from least-squares fits to frequency kernels obtained with sum-of-sinusoids test stimuli with monochromatic (477 nm) light at $I_0 = 10^{-4}$ W m^{-2}.

The Q_{10} is expected to be about unity for temperature independent processes (e.g., purely physical processes such as diffusion), and greater than 2 for enzymatic reactions (Nobel, 1983). The present value of 1.6 suggests that the latency may be due to a combination of chemical cascades and diffusion. With the above limits of Q_{10} for enzymatic reactions, we estimate that between 1 and 2 min of the latency may be due to physical processes, such as diffusion, which have very weak dependence on temperature.

Nonlinear Analysis

The nonlinear subsystem of the model (Fig. 4 *b* of Pratap et al., 1986) contains a squarer S preceded by a second-order low-pass filter P_1 in parallel with a high-pass filter P_2. Although the squarer itself is a static nonlinear device, the two filters make the overall nonlinearity dynamic. The damping coefficient α_{N1} of the second-order low-pass filter is approximately unity at all wavelengths. As in the previous paper, this filter can therefore be factored into two identical first-order low-pass filters.

The gain factors (β_{N1} and β_{N2}) of the two filters in the nonlinear subsystem depend on wavelength. Both have peaks at 487 nm. The gain factor β_{N1} of the low-pass filter indicates how much this filter contributes to the second-order kernels at different wavelengths; the larger the gain factor, the more nonlinear the system. Therefore, the system should be more nonlinear at 487 nm than at 446 nm. We see this feature reflected in Table I, where the strength of nonlinearity and the percentage improvement of the second-order model over the first-order model are both large for 487 nm. The connection between the gain factor of the high-pass filter (β_{N2}) and the degree of nonlinearity is not as clear, because both the gain factor and the cutoff frequency f_{N2} depend on wavelength; the transfer function of the high-pass filter is directly proportional to the gain factor, but decreases as the cutoff-frequency parameter f_{N2} increases.

Conclusion

In the previous paper, we interpreted the wild-type kernel (at 10^{-4} W m^{-2}, 477 nm, and 20°C) with a model consisting of several filters and a static nonlinear element. These filters represent the rate-limiting steps and other slow processes that fall within the bandwidth of the response. The results of this paper indicate that some of these slow processes depend on wavelength, and thus may be associated with the photoreceptor system.

From the wavelength dependence of the latency, we have placed an upper limit of ~3.4 min on the contribution of Type 1 delays. From the temperature dependence of the latency, we have estimated that 1–2 min of the latency may be due to physical processes (which result in Type 1 delays). The remaining 2–2.5 min of latency are probably due to chemical reactions in the system (Type 2 delays), each of which alone is probably faster than the rate-limiting step, and therefore cannot be readily distinguished. From the wavelength dependence of the latency, we had placed a lower limit of 1.3 min on the contribution of Type 2 delays to the latency. These two separate estimates of the relative contributions of Type 1 and Type 2 delays to the latency are consistent.

Recent evidence indicates that the light responses in *Phycomyces* are mediated by multiple interacting photoreceptors (Galland et al., 1984; Galland and Lipson, 1985*a*, *b*). Our work supports this hypothesis because it shows that several processes in the light-growth response system depend on wavelength.

We thank Paul Galland and Benjamin Horwitz for valuable discussions and for critical reading of the manuscript.

This work was supported by grant GM29707 from the National Institutes of Health to Edward D. Lipson.

Received for publication 24 January 1986.

REFERENCES

Bergman, K., A. P. Eslava, and E. Cerda-Olmedo. 1973. Mutants of *Phycomyces* with abnormal phototropism. *Mol. Gen. Genet.* 123:1–16.

Bowles, D. J., and D. H. Northcote. 1974. The amounts and rates of export of polysaccharides found within the membrane system of maize root cells. *Biochem. J.* 142:139–144.

Capellos, C., and B. H. J. Bielski. 1972. Kinetic Systems. Mathematical Description of Chemical Kinetics in Solution. Wiley-Interscience, New York. 49–51.

Delbrück, M., and W. Reichardt. 1956. System analysis for the light-growth response of *Phycomyces*. *In* Cellular Mechanisms in Differentiation and Growth. D. Rudnick, editor. Princeton University Press, Princeton, New Jersey. 3–44.

Delbrück, M., and W. Shropshire. 1960. Action and transmission spectra of *Phycomyces*. *Plant Physiol.* 35:194–204.

Foster, K. W., and E. D. Lipson. 1973. The light growth response of *Phycomyces*. *J. Gen. Physiol.* 62:590–617.

French, A. S. 1980. The linear dynamic properties of phototransduction in the fly compound eye. *J. Physiol. (Lond.).* 308:385–401.

Fuortes, M. G. F., and A. L. Hodgkin. 1964. Changes in time scale and sensitivity in the ommatidia of *Limulus*. *J. Physiol. (Lond.).* 172:239–263.

Galland, P., and E. D. Lipson. 1985*a*. Action spectra for phototropic balance in *Phycomyces blakesleeanus:* dependence on reference wavelength and intensity range. *Photochem. Photobiol.* 41:323–329.

Galland, P., and E. D. Lipson. 1985*b*. Modified action spectra of photogeotropic equilibrium in *Phycomyces blakesleeanus* mutants with defects in genes *madA*, *madB*, *madC*, and *madH*. *Photochem. Photobiol.* 41:331–335.

Galland, P., A. S. Pandya, and E. D. Lipson. 1984. Wavelength dependence of dark adaptation in *Phycomyces* phototropism. *J. Gen. Physiol.* 84:739–751.

Galland, P., and V. E. A. Russo. 1984. Light and dark adaptation in *Phycomyces* phototropism. *J. Gen. Physiol.* 84:101–118.

Lipson, E. D. 1975*a*. White noise analysis of *Phycomyces* light growth response system. I. Normal intensity range. *Biophys. J.* 15:989–1012.

Lipson, E. D. 1975*b*. White noise analysis of *Phycomyces* light growth response system. II. Extended intensity ranges. *Biophys. J.* 15:1013–1032.

Lipson, E. D., and S. M. Block. 1983. Light and dark adaptation in *Phycomyces* light-growth response. *J. Gen. Physiol.* 81:845–859.

Nobel, P. S. 1983. Biophysical Plant Physiology and Ecology. Freeman Publications, San Francisco, CA. 49–51.

Poe, R. C., and E. D. Lipson. 1986. System analysis of *Phycomyces* light-growth response with Gaussian white noise test stimuli. *Biol. Cybern.* In press.

Pratap, P. R., A. Palit, and E. D. Lipson. 1986. System analysis of *Phycomyces* light-growth response with sum-of-sinusoids test stimuli. *Biophys. J.* 50:000–000.

Ray, P. M. 1977. Auxin-binding sites of maize coleoptiles are localized on membranes of the endoplasmic reticulum. *Plant Physiol.* 59:594–599.

Robinson, D. G., and U. Kristen. 1982. Membrane flow via the Golgi apparatus of higher plants. *Int. Rev. Cytol.* 77:89–95.

Thornton, R. M. 1968. The fine structure of *Phycomyces* II. Organization of the stage I sporangiophore apex. *Protoplasma.* 66:269–285.

Victor, J. D., and R. M. Shapley. 1980. A method of nonlinear analysis in the frequency domain. *Biophys. J.* 29:459–484.